Superconductivity and magnetism of a body-centered tetragonal $ErRh_4B_4$ single crystal. I. Metamagnetism under the fourfold magnetic anisotropy

H. Iwasaki, M. Ikebe, and Y. Muto
The Research Institute for Iron, Steel and Other Metals, Tohoku University, Sendai 980, Japan
(Received 14 August 1985)

Magnetization was measured on a single crystal of body-centered tetragonal $ErRh_4B_4$, an antiferromagnetic superconductor. It was found that the c axis is the strong hard-magnetization direction. A large fourfold magnetic anisotropy was observed in the tetragonal c plane. The [100] and [010] axes are the easy-magnetization directions and the [110] axis is the hard-magnetization one in the c plane. The magnetization curves below T_N show two-step jumps in both cases of $\mathbf{H}||[100]$ and $\mathbf{H}||[010]$ and show only one-step jumps in the case of $\mathbf{H}||[110]$. Furthermore, it is shown that superconductivity coexists with intermediate magnetic states under a magnetic field in the c plane. The magnetization process in the c plane is understood as metamagnetism and can be explained by a four-sublattice model taking account of the fourfold magnetic anisotropy. Based on the fact that Er spins are approximately located on an fcc lattice in bct $ErRh_4B_4$, the type of the antiferromagnetic order is discussed. The two-step jump in the magnetization for $\mathbf{H}||[100]$ indicates that the magnetic structure belongs to the first-kind ordering in the antiferromagnetic fcc lattice. The magnetization process below T_N is discussed, and the exchange constants between the magnetic spins are determined. The results obtained are consistent with the stability condition of the first-kind ordering.

I. INTRODUCTION

Ternary rare-earth compounds $\mathscr{R}Rh_4B_4$ ($\mathscr{R}$ is a rare-earth metal) have been given intense attention[1] since their discovery. Many experimental and theoretical studies[2] have been actively done on these materials which exhibit a wide variety of unusual behaviors caused by the interplay between superconductivity and long-range magnetic order.

Among them, $ErRh_4B_4$ with a primitive tetragonal (pt) structure[3] is a typical ferromagnetic superconductor and shows a reentrant behavior, where superconductivity with $T_c=8.7$ K is quenched by an occurrence of a ferromagnetic order at $T_M=0.9$ K. Furthermore, according to a recent neutron-diffraction experiment[4] on a single-crystal sample, a magnetic order with a long wavelength of about 100 Å appears in a narrow temperature range just above the ferromagnetic ordering temperature, coexisting with superconductivity, where this order is a spin-sinusoidal order. This occurs surely as a result of competition between superconductivity and ferromagnetic order.[5,6]

Recently we found that $ErRh_4B_4$ with a body-centered tetragonal (bct) structure also exists as an antiferromagnetic superconductor.[7] The bct $\mathscr{R}Rh_4B_4$ compounds can be synthesized for some rare-earth elements. According to Johnston,[8] the bct phase is easily stabilized in an $\mathscr{R}(Rh_{1-x}Ru_x)_4B_4$ system, where Rh atoms are partially substituted by Ru atoms. Several studies on the bct $\mathscr{R}(Rh_{1-x}Ru_x)_4B_4$ system have been made on polycrystalline samples.[9–12] Magnetic order of this system changes from the antiferromagnetic to the ferromagnetic order as Rh atoms are replaced by Ru ones. In the Rh-rich region the antiferromagnetic order coexists with superconductivity below the Néel temperature T_N.

As the magnetic order temperature is very low in the magnetic superconductors such as bct $ErRh_4B_4$, it is expected that the exchange interaction between magnetic ions is extremely small. Metamagnetism, which appears when the magnetic anisotropy energy is larger than the exchange energy, may be easily observable. Magnetic anisotropy may also play an important role in superconducting properties. However, such an anisotropy effect has not been observed because of the difficulty in obtaining a single-crystal sample. In particular, there is no report of a single crystal in any antiferromagnetic superconductor.

Recently, we have succeeded in preparing a bct $ErRh_4B_4$ single crystal. In the present paper we report and discuss the metamagnetism in the tetragonal c plane which is observed in the bct $ErRh_4B_4$ single crystal. Furthermore, we describe the coexistence of superconductivity and magnetic order under a magnetic field. In Sec. II the experimental procedure is briefly described. In Sec. III the crystal structure of bct $ErRh_4B_4$ is described in comparison with that of pt $\mathscr{R}Rh_4B_4$ and the experimental results are presented in Sec. IV. In Sec. V fourfold magnetic anisotropy in the c plane is discussed. Magnetic free energy is given and magnetic structures which explain observed metamagnetism are proposed. Finally, the analysis of the experimental results are given. Anisotropy of the upper critical field will be separately discussed in the following paper,[13] referred to as paper II. Three brief papers on various properties of this single crystal were already published elsewhere.[14–16]

II. EXPERIMENTAL

The bct $ErRh_4B_4$ single crystal was synthesized by an induction heating technique. All of the elements were of 99.9% purity. The sample was obtained by three steps.

(i) Mixed powder of Rh and B was pressed into a pellet. It was sealed into a quartz tube under Ar atmosphere and then sintered at 1050°C for two days in order to obtain the binary compound RhB. (ii) The sintered RhB was melted together with Er ingots by induction heating under an Ar atmosphere. The bct $ErRh_4B_4$ ingot obtained consisted of several small single crystals. (iii) A rather large single crystal was cut out of the ingot, where its crystal orientation was confirmed by means of the back-reflection Laue method. The sample has a dimension $1.95 \times 1.25 \times 0.5$ mm^3. The sample shape implies that the demagnetization coefficient is large along the [001] axis and small in the c plane.

The magnetization above 1.7 K was measured by a vibrating sample magnetometer. Ni with 99.99% purity was used as a standard sample in order to calibrate the absolute value of magnetization. The magnetization below 1.3 K was measured by integrating a dc-induced voltage of a compensated two-coil system when a magnetic field was swept. Electrical resistance and ac magnetic susceptibility were measured by an ac or dc four-probe and a mutual-inductance method, respectively. A ^{3}He-^{4}He dilution refrigerator was used for the measurement below 1.3 K.

III. CRYSTAL STRUCTURE OF bct $ErRh_4B_4$

In order to make descriptions of the experimental results clear, the crystal structure of bct $ErRh_4B_4$ is first discussed. The bct $ErRh_4B_4$ compound belongs to the crystal structure of the $LuRu_4B_4$ type which is a body-centered tetragonal with $c/a \lesssim 2$. In Fig. 1(a) is shown schematically the crystal structure of the $LuRu_4B_4$ type, while in Fig. 1(b) is shown that of the $CeCo_4B_4$ type for comparison, to which primitive tetragonal $\mathscr{R}Rh_4B_4$ such as pt $ErRh_4B_4$ belongs. It can be seen that both crystal structures are very similar to each other. The $LuRu_4B_4$-type structure was studied by Johnston[8] on $\mathscr{R}(Rh_{0.85}Ru_{0.15})_4B_4$ as well as on $\mathscr{R}Ru_4B_4$ and was found to be a new structure type. The basic building blocks of the bct structure are the same as in the $CeCo_4B_4$-type phase. In both structures, the T_4B_4 clusters (T is transition metal) and rare-earth (RE) atoms are set in a NaCl-type array, where RE atoms are arranged in slightly distorted fcc positions. The distance between the two nearest RE atoms is almost the same in both structures. There are two kinds of T_4B_4 units with the different orientations in both structures, as shown in Fig. 1(c). While the T_4B_4 units with the same orientation in the $CeCo_4B_4$ type are arranged into sheets perpendicular to the c axis [Fig. 1(b)], they are distributed equally in each plane in an ordered way in the $LuRu_4B_4$ type, as shown in Fig. 1(a). The smallest distance between T atoms belonging to different T_4B_4 units occurs between tetrahedra of the same orientation in adjacent c planes rather than within the c plane. This smallest distance is comparable to that between T atoms in the same tetrahedron.

Whereas the RE atoms form the slightly distorted fcc lattice in bct $ErRh_4B_4$, the T_4B_4 units do not form the fcc lattice because the two kinds of those with different orientations exist in these compounds. Therefore, in bct $ErRh_4B_4$, the fourfold symmetry holds in the c plane and the twofold symmetry holds in the a plane. The smallest distance between RE atoms in the same c plane is slightly larger than that between neighboring c planes.

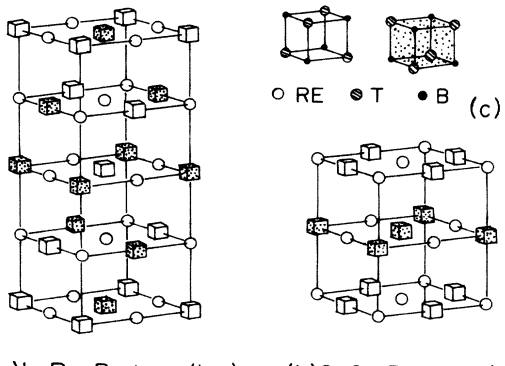

FIG. 1. Schematic crystal structures of both the (a) $LuRu_4B_4$ type and (b) $CeCo_4B_4$ type. For clarity the cubes representing the Rh_4B_4 units are not drawn to scale. (c) T_4B_4 units with different orientations.

IV. EXPERIMENTAL RESULTS

Figure 2 shows the temperature dependence of the electrical resistance R and that of the ac magnetic susceptibility χ_{ac} near T_c. The superconducting transition temperature T_c is defined by linear extrapolation of R to zero. This temperature almost coincides with the temperature at which the diamagnetic χ_{ac} becomes perceptible at first. The transition width is 30 mK. The residual resistivity ρ_0

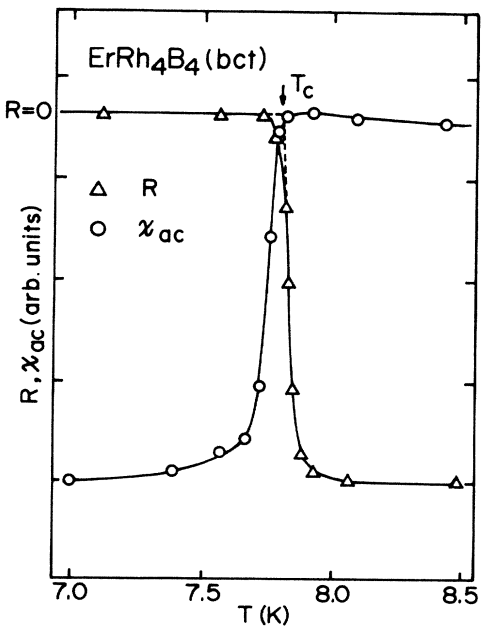

FIG. 2. Temperature dependence of electrical resistance R and ac susceptibility χ_{ac} near T_c. T_c is defined by linear extrapolation of R to zero

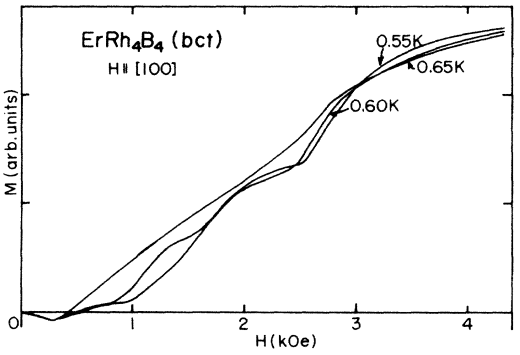

FIG. 3. Magnetization curves for $\mathbf{H}\|[100]$ near T_N, where T_N is defined.

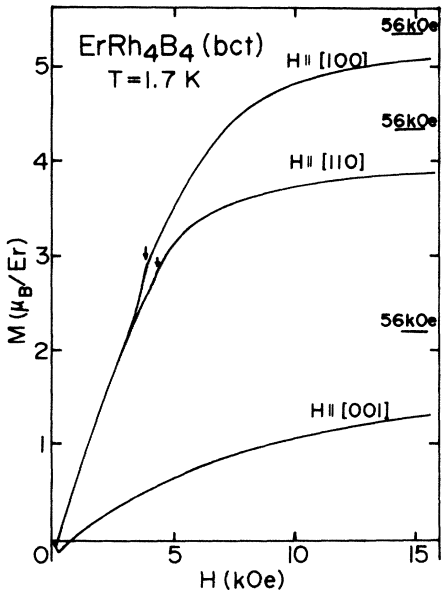

FIG. 4. Magnetization curves for $\mathbf{H}\|[100]$, $\mathbf{H}\|[110]$, and $\mathbf{H}\|[001]$ at 1.7 K. The magnetizations at 56 kOe are marked at the right-hand side. The field at which the magnetization has its kink is shown by the arrow.

and the residual resistance ratio (RRR) are $\sim 65\ \mu\Omega$ cm and 1.70, respectively.

It is very difficult to determine precisely T_N from only the magnetization measurements when superconductivity and antiferromagnetic order coexist as in bct $ErRh_4B_4$. Figure 3 shows the magnetization near T_N along the [100] direction. Jumps in the magnetization curves are observed in low-temperature data, which will be discussed soon. T_N is defined as being 0.65 K, where such a structure disappears. This temperature is a little higher than 0.6 K, at which the $H_{c2}(T)$ curve in the [100] axis takes a minimum.[15] (See paper II.)

Figure 4 shows magnetization curves along the [100], [110], and [001] directions at 1.7 K, where the sample is in the superconducting paramagnetic state. The perfect diamagnetism is initially observed when a magnetic field is applied along each direction. Since the magnetization along the [001] direction is very small, the c axis is the hard-magnetization direction. Magnetizations along both the [100] and [110] directions coincide with each other in lower fields. In higher fields, the magnetization along the [100] direction is considerably larger than that along the [110] direction, since the latter is strongly suppressed. Thus, the [100] axis is the easy-magnetization direction. The arrows in Fig. 4 are the fields at which the magnetizations show kinks in both directions, which are almost in agreement with H_{c2} determined by resistive measurements.[14] It should be noted that in this field range the effect of magnetic anisotropy becomes clearly detectable in the magnetization curves. The magnetizations along the [010] and [1$\bar{1}$0] directions almost coincide with those along the [100] and [110] directions, respectively, though they are not shown here. It is very important that the magnetization in the c plane show the fourfold symmetry which reflects the crystal structure of bct $ErRh_4B_4$. It should be added that no kink appears for the [001] direction but H_{c2} is very large (43 kOe at 1.7 K).

The magnetization values at 56 kOe along the [100], [110], and [001] directions are $5.3\mu_B$, $4.4\mu_B$, and $2.2\mu_B$ per Er, respectively, as marked on the right-hand side of Fig. 4. The magnetization along the [100] direction is almost saturated in this field.

Figures 5(a), 5(b), and 5(c) show magnetization curves at 0.1, 0.5, 0.7, and 1.3 K along the [100], [010], and [110] directions, respectively. Though the magnetization curves above T_N are qualitatively similar for every direction, those below T_N along the [100] and [010] directions are quite different from those along the [110] one. The magnetization below T_N shows a two-step jump when a magnetic field is applied along the [100] and [010] directions, as seen in Figs. 5(a) and 5(b). H_1 and H_3 are defined at the midpoint values of the first and the second jump, respectively. The magnetization curves in increasing and decreasing fields are different so that a large hysteresis of the magnetization appears. [See the curve at 0.1 K in Fig. 5(a).] Especially, the hysteresis at H_1 is very large. Though the field range over the jump is wide at 0.5 K just below T_N, it becomes narrower with decreasing temperatures. An intermediate ferrimagnetic state appears in the field range between H_1 and H_3, where the magnetization value is half of the saturation value M_0 of the induced ferromagnetic state appearing above H_3. Though the magnetization curve for a virgin state is shown in Figs. 5(a), 5(b), and 5(c), a similar magnetization curve reappears in the second run.

The magnetization curves along the [100] and [010] directions are not identical, but both values of H_1 and H_3 in the case of $\mathbf{H}\|[010]$ [Fig. 5(b)] are larger than those in the case of $\mathbf{H}\|[100]$ [Fig. 5(a)]. Such discrepancy is also observed in the upper critical field H_{c2}. (See paper II.) H_{c2} along the [010] direction is larger than that in the case of $\mathbf{H}\|[100]$ in the antiferromagnetic superconducting state.[15] (The same result is also obtained in the paramagnetic superconducting state.) It is important to note that this discrepancy observed in both magnetization and H_{c2} is beyond the demagnetization correction. Therefore, there is actually a small difference in the magnetic

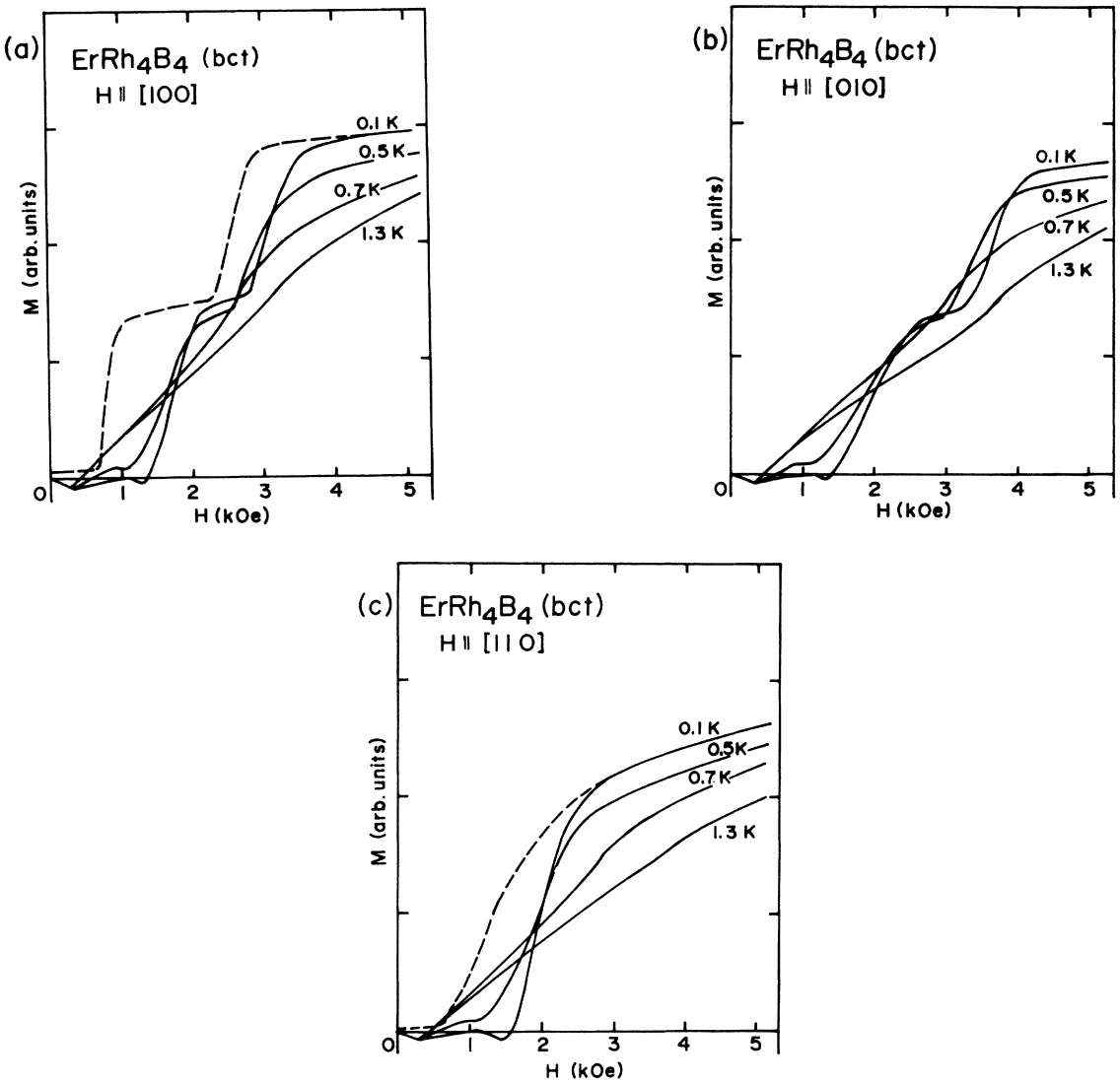

FIG. 5. Magnetization curves in the c plane below 1.3 K. (a) $\mathbf{H}\|[100]$, (b) $\mathbf{H}\|[010]$, and (c) $\mathbf{H}\|[110]$. Solid and dashed curves show the magnetizations for increasing and decreasing fields, respectively.

anisotropy between the [100] and [010] directions, though both directions are crystallographically equivalent. We believe that the difference might originate from an imperfection within the sample.

The magnetization curve along the [110] direction in Fig. 5(c) shows a one-step jump at H_2 with a large hysteresis in increasing and decreasing fields, as exemplified by the curve at 0.1 K, where H_2 is a midpoint of the jump. The magnetization after the jump takes a value (about $M_0/\sqrt{2}$) between $M_0/2$ and M_0 and then increases gradually as a magnetic field increases. The magnetization process in the c plane below T_N is understood as metamagnetism under the fourfold magnetic anisotropy, as will be discussed later in detail.

Figure 6 shows H_1 and H_3 for the [100] direction and H_2 for the [110] one as a function of the temperature for both increasing and decreasing fields. These H_i ($i=1-3$) values depend somewhat on temperature. When we take ΔH_i as a magnitude of hysteresis, we obtain $\Delta H_1=1.0$, $\Delta H_2=0.9$, and $\Delta H_3=0.6$ kOe at 0 K. It is concluded that these jumps are the phase transition of the first order. It should be remembered that $H_3/H_1\simeq 2.3$ when the mean values of H_i for both increasing and decreasing fields are taken at 0 K.

It is now clear that in bct $ErRh_4B_4$, superconductivity coexists with antiferromagnetic order below T_N at $H=0$. The magnetization decreases once with increasing field in the field range just below H_1 and H_2, as seen in Figs. 5(a), 5(b), and 5(c). In this field range, the sample is surely in the mixed state. This anomaly is observed only below T_N and it is not observed in a field range just below H_3. It is observed only for increasing field. This anoma-

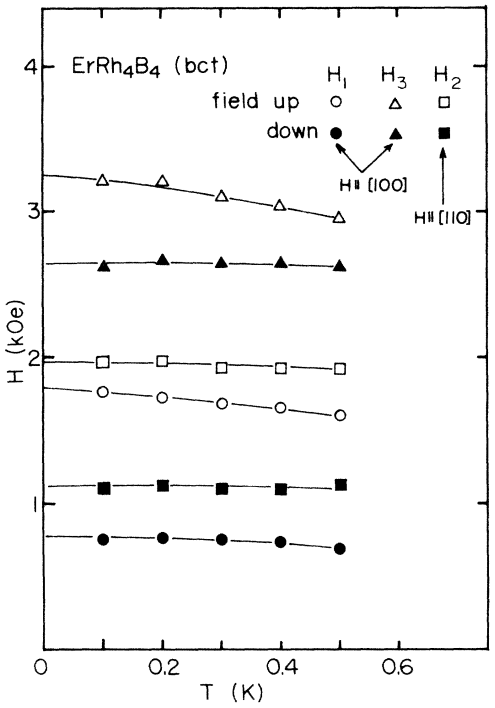

FIG. 6. Temperature dependence of H_1 and H_3 for $\mathbf{H}\|[100]$ and H_2 for $\mathbf{H}\|[110]$. Open and solid symbols show H_i ($i=1,2,3$) for increasing and decreasing fields, respectively.

ly seems to be caused by the interplay between superconductivity and magnetism because this anomaly is observed in the superconducting mixed state. When the data for increasing fields in Figs. 5(a), 5(b), and 5(c) are converted to the magnetic induction versus magnetic field curves, as can be clearly seen in Figs. 7(a) and 7(b), it becomes clear that the magnetic induction is almost constant in the field range in which the anomalous magnetization takes place. This means that the number of vortices is almost constant there. The origin of this anomaly is interpreted as follows. In the mixed state, the local magnetic field fluctuates spatially in the sample. The metamagnetic transition

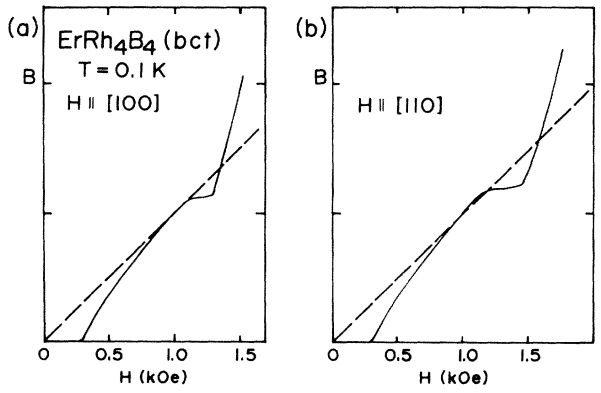

FIG. 7. Magnetic induction versus magnetic field curves at 0.1 K (a) for $\mathbf{H}\|[100]$ and (b) for $\mathbf{H}\|[110]$.

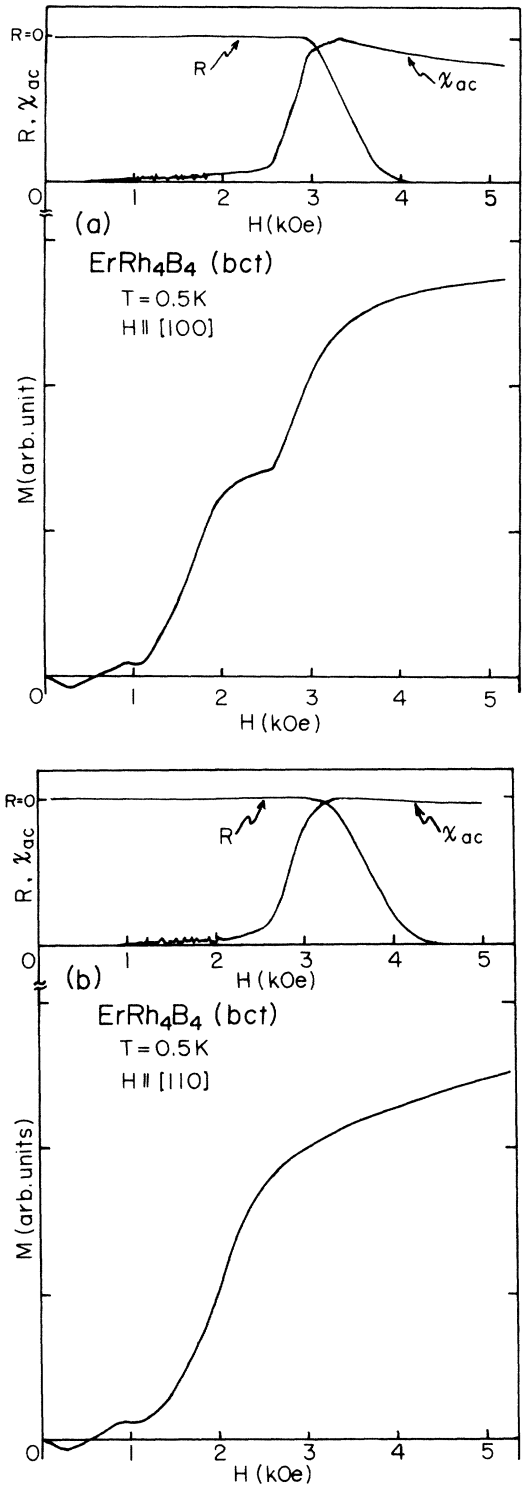

FIG. 8. Magnetization, electrical resistance, and ac susceptibility versus magnetic field curves at 0.5 K (a) for $\mathbf{H}\|[100]$ and (b) $\mathbf{H}\|[110]$. Noise between 1 and 2 kOe is a signal which corresponds to the metamagnetic transition in each case.

is initially caused in the vortex core, because the local field takes a maximum there. The exchange energy in the core is increased by the metamagnetic transition. It is explained by the free-energy analysis that a state in which the vortex density keeps constant is stabilized by this ener-

gy increase. As a result, the entrance of the vortex is suppressed and the magnetic induction remains constant. The detailed mechanism of this anomalous phenomenon was discussed in a separate paper.[16]

Next we describe the coexistence between superconductivity and ferrimagnetic order under a magnetic field. A ferrimagnetic order with magnetization of $M_0/2$ appears as an intermediate state for $\mathbf{H}||[100]$ or $\mathbf{H}||[010]$. In Fig. 8(a) the electrical resistance, the ac susceptibility, and the magnetization at 0.5 K are shown as a function of magnetic field. The ac susceptibility indicates that superconductivity begins to be destroyed at the field where the second jump in the magnetization occurs. Therefore, superconductivity coexists with the intermediate ferrimagnetic state between H_1 and H_3 for $\mathbf{H}||[100]$. The same result is obtained for $\mathbf{H}||[010]$.

In Fig. 8(b) the electrical resistance, the ac susceptibility, and the magnetization at 0.5 K are shown as a function of a magnetic field along the [110] direction. In this case the phase transition from an antiferromagnetic to a canted ferromagnetic state occurs at H_2 as will be discussed later. It can be seen that superconductivity begins to be destroyed at higher fields than H_2, as seen in ac susceptibility and the electrical resistance data. Therefore, we conclude that the canted ferromagnetic order with $M_0/\sqrt{2}$ also coexists with superconductivity for $\mathbf{H}||[110]$.

V. DISCUSSION

A. Fourfold magnetic anisotropy in the c plane

From the magnetization curves in the paramagnetic phase of bct $ErRh_4B_4$, it is clear that the easy-magnetization direction is the [100] axis and the hard-magnetization direction is the [001] axis (Fig. 4). Moreover, it is found that the large fourfold magnetic anisotropy exists in the c plane. The origin of the magnetic anisotropy is considered to come from the crystalline electric field.

1. Anisotropy of the magnetic susceptibility above T_N

The angular dependence of the magnetic susceptibility in the paramagnetic state is given by

$$\chi(\theta)=\chi_{[100]}\cos^2\theta+\chi_{[010]}\sin^2\theta\ , \tag{1}$$

where θ is measured from the [100] axis. Because the [010] axis should be equivalent to the [100] axis, we can express it as $\chi_{[100]}=\chi_{[010]}\equiv\chi$. Thus, Eq. (1) is rewritten as

$$\chi(\theta)=\chi(\cos^2\theta+\sin^2\theta)=\chi\ . \tag{2}$$

It should be noted from Eq. (2) that there appears no anisotropy of the magnetic susceptibility (=low-field magnetization) in the paramagnetic state, even if the large fourfold magnetic anisotropy exists in the c plane. The effect of the fourfold magnetic anisotropy should appear in higher fields in which Er spins arrange in the direction of an applied field. The magnetization curves in the [100] and [110] directions in Fig. 4 typically show these characteristics.

2. Magnetization process below T_N

The magnetization process in an antiferromagnet with a uniaxial magnetic anisotropy is divided into two cases, depending on the relative magnitude of the magnetic anisotropy energy E_A to the exchange energy E_E. It is well known that in the case of $E_A>E_E$ the magnetization process shows metamagnetism and in the case of $E_A<E_E$ it shows the spin-flop transition.

When the fourfold magnetic anisotropy exists, E_A corresponds to the energy difference of the magnetic anisotropy between the [100] axis, which is the easy-magnetization direction, and the [110] axis, which is the hard-magnetization direction in the c plane. In the antiferromagnetic state there are two kinds of magnetic domains where magnetic spins arrange along the [100] and [010] axes. It should be noted in the metamagnetic case ($E_A>E_E$) that a magnetic structure, in which the magnetic spins make a right angle to one another, can appear as an intermediate state. This structure does not appear in the uniaxial magnetic anisotropy but is characteristic in the fourfold magnetic anisotropy.

B. Magnetization process and four-sublattice model

The magnetization process in the tetragonal c plane of bct $ErRh_4B_4$ is explained as metamagnetism under the fourfold magnetic anisotropy. As can be seen in Figs. 5(a) and 5(b), the magnetization curves along the [100] and [010] axes show two-step jumps accompanied by a hysteresis for increasing and decreasing fields, and the magnetization of an intermediate state is half of the saturation moment $M_0/2$. In addition, the magnetization curves differ a little between the cases of $\mathbf{H}||[100]$ and $\mathbf{H}||[010]$. On the other hand, as can be seen in Fig 5(c), the magnetization curve along the [110] axis shows a one-step jump at H_2 accompanied by a hysteresis for increasing and decreasing fields, where the magnetization value just after the jump is $M_0/\sqrt{2}$.

These experimental results are explained by a four-sublattice model as follows. In Fig. 9 is schematically shown the magnetic structures in a four-sublattice model under a magnetic field along the [100], [010], and [110] directions, where AF, I, and F express antiferromagnetic, intermediate, and induced ferromagnetic states. In the cases of $\mathbf{H}||[100]$ and $\mathbf{H}||[010]$, two kinds of magnetic structures with $M_0/2$, I_1, and I_2 which are degenerate to each other can exist as intermediate ferrimagnetic states. When a magnetic field further increases, finally all of the magnetic spins array along a magnetic field. When a magnetic field is applied along the [110] direction, a canted ferromagnetic order in which the two sublattices are arranged along the [100] direction and the others along the [010] direction appears as an intermediate state. The magnetization of this structure is $M_0/\sqrt{2}$. Directions of the moments gradually rotate toward the [110] direction with increasing magnetic field, attaining finally the induced ferromagnetic state.

The jumps at H_1 and H_3 observed in bct $ErRh_4B_4$ for $\mathbf{H}||[100]$ correspond to the phase transitions from the antiferromagnetic to the ferrimagnetic ordered state (I_1 or I_2) with the magnetization of $M_0/2$ and from the ferri-

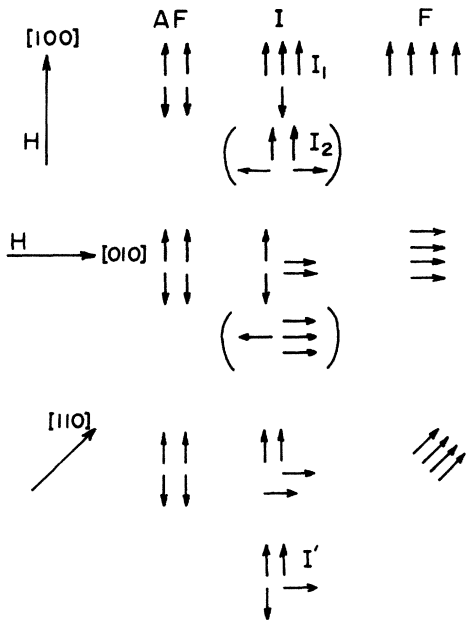

FIG. 9. Schematic magnetic structures under a magnetic field for H||[100], H||[010], and H||[110]. See text about the terms AF, I_1, I_2, F, CF, and I'.

magnetic to the induced ferromagnetic ordered state, respectively. The magnetization process for H||[010] is similar to that for H||[100]. If the experimental result that the small energy difference of the magnetic anisotropy between the [100] and [010] axes actually exists is considered, the magnetic anisotropy for the spins along the [100] axis is smaller than that for the spins along the [010] one. Therefore, the free energy for the I_1 state is slightly lower than that for the I_2 state by the small energy difference of magnetic anisotropy. Thus, the I_1 and I_2 states appear as the ferrimagnetic state for H||[100] and H||[010], respectively.

The jump at H_2 for H||[110] corresponds to the phase transition from the antiferromagnetic to the canted ferromagnetic (CF) order with the magnetization of $M_0/\sqrt{2}$. The free-energy analysis given in the following section indicates that a magnetic structure I' may also appear in the case of H||[110], as shown in the bottom of Fig. 9. This magnetic structure has the magnetization of $M_0/2\sqrt{2}$, which is not observed in our experiments.

C. Magnetic free energy at 0 K and its correction of contributions of superconductivity

When the magnetic free energy of an antiferromagnet is discussed, it consists of exchange energy, magnetic anisotropy energy, and Zeeman energy. The magnetic anisotropy energy need not be considered in this case, because the magnetic spins are always along the [100] and [010] axes of easy magnetization in every magnetic structure. Though the small energy difference of the magnetic anisotropy is observed between the [100] and [010] axes, it may be neglected in the calculation of the magnetic free energy. It is assumed that the contribution of this difference only appears in discussing proposed magnetic structures. Details will be described in the following Sec. V D.

The effective field H_{eff} consists of the external magnetic field, the Lorentz local field ($4\pi\mathbf{M}/3$), and the demagnetization field ($-n\mathbf{M}$). Because the Er spin has a large magnetic moment, the Lorentz local field cannot be neglected. Thus, the magnetic free energy E is written as the sum of the exchange energy and the Zeeman energy in which the effective field is taken into account as follows:

$$E=-\sum \mathcal{J}_{ij}(g_J-1)^2\mathbf{J}_i\cdot\mathbf{J}_j-\sum \boldsymbol{\mu}_i\cdot(\mathbf{H}+4\pi\mathbf{M}/3-n\mathbf{M}) , \tag{3}$$

where $\boldsymbol{\mu}_i$ and $\mathbf{J}_i$ are the magnetic moment and the total angular momentum of the ith Er ion, respectively, and g_J is the Landé g factor. $\mathcal{J}_{ij}$ is the exchange constant between the ith and the jth Er spins. The demagnetization term nM can be neglected because it is small in the c plane on this sample, as mentioned in Sec. II.

Superconductivity can coexist with the antiferromagnetic state. In Sec. IV it has become clear that superconductivity also coexists with the intermediate ferrimagnetic state for H||[100] and H||[010] and with the canted ferromagnetic state for H||[110] under a magnetic field. Therefore, in advance of the magnetic free-energy analysis we must take account of the contribution of the superconducting condensation energy to the magnetic free energy. It should be noticed that because of the contribution of the superconducting condensation energy, H_1, H_2, and H_3 observed in our experiments are higher than those of hypothetical bct $ErRh_4B_4$ which do not show superconductivity. In order to make a correction to the condensation energy, the following rough consideration is needed.

As will be discussed in paper II, the spin polarization due to the s-f exchange interaction AM^2 is the most decisive pair-breaking mechanism to determine H_{c2} in the c plane. In the presence of spin-orbit scattering, the relative rise ΔE of the energy due to the spin paramagnetic pair breaking is given as follows:

$$(\chi_n-\chi_s)H^2/2=\Delta E , \tag{4}$$

where χ_n and χ_s are the spin susceptibility in the normal and the superconducting states, respectively. H^2 in Eq. (4) can be replaced by AM^2 when the spin polarization effect due to the s-f exchange interaction is decisively large. We roughly try to estimate the superconducting condensation energy for each magnetic state.

Because in the antiferromagnetic state the net magnetic moment is zero, the superconducting condensation energy is fully retained. In the induced ferromagnetic state the superconducting condensation energy is zero because superconductivity is quenched in this state. Although for H||[110], superconductivity coexists with the canted ferromagnetic state, it is quenched at the field just above the metamagnetic transition field H_2. Therefore, the superconducting condensation energy is nearly equal to zero in this state with $M_0/\sqrt{2}$. Then the superconducting condensation energy E_0 of bct $ErRh_4B_4$ is estimated as follows:

$$E_0=(\chi_n-\chi_s)A(M_0/\sqrt{2})^2/2 . \tag{5}$$

The superconducting condensation energy in the ferrimagnetic state with $M_0/2$ for H||[100] is written as

$$E_0-(\chi_n-\chi_s)A(M_0/2)^2/2=E_0/2\ . \tag{6}$$

Thus, the free energies in the antiferromagnetic and ferrimagnetic states are lowered by E_0 and $E_0/2$, respectively, from that of hypothetical bct $ErRh_4B_4$ which does not show superconductivity.

The corrections to H_1 and H_3 are schematically explained by Figs. 10(a) and 10(b). E_0 is estimated from the magnetization curve at 0.7 K just above T_N, as can be understood by Fig. 10(a). H_1 and H_3 are lowered by the same amount of the field which corresponds to $E_0/2$. The shifts of H_1 and H_3 are estimated to be both about 150 Oe. In Fig. 10(b) the solid curve shows the experimental magnetization and the dashed curve shows the magnetization after the correction of the superconducting condensation energy. As mentioned in Sec. IV, the metamagnetic transition fields H_i $(i=1-3)$ show hysteresis between increasing and decreasing fields. In the free-energy analysis the midpoint of the values for increasing and decreasing fields is taken as H_i. After the corrections, the metamagnetic transition fields become $H_1=1150$ Oe and $H_3=2800$ Oe at 0 K, and then the ratio, $H_3/H_1=2.4$. Because the corrected values of H_1 and H_3 are obtained, we can proceed with our discussion on the magnetization process on the basis of Eq. (3).

D. Magnetic structures of bct $ErRh_4B_4$

According to Smart,[17] when the exchange constant $\mathcal{J}$ between nearest neighbors and the exchange constant $\mathcal{J}'$ between second-nearest neighbors are considered, three kinds of antiferromagnetic structures can be expected in the fcc lattice. Furthermore, Kanamori[18] advanced a theoretical study on the magnetization process in an Ising spin system with cubic symmetry. In Fig. 11 are shown magnetic structures in the fcc lattice clarified by him as functions of $\mathcal{J}$ and $\mathcal{J}'$. Besides the ferromagnetic case, the magnetic structures in the fcc lattice are divided into three kinds of antiferromagnetic structures. These are called the first-, second-, and third-kind ordering and are expressed as cases I, II, and III in Fig. 11, respectively.

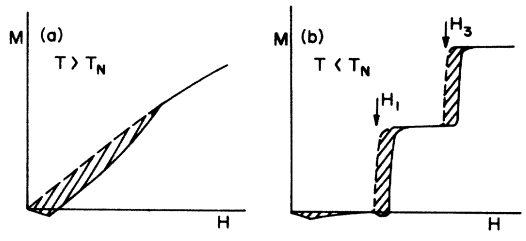

FIG. 10. (a) Schematic magnetization curve just above T_N. Superconducting condensation energy E_0 is shown by the hatched area. The dashed curve is magnetization of the normal state. (b) Schematic magnetization curve below T_N. The solid curve shows the experimental magnetization and the dashed curve shows the magnetization after correction of the superconducting condensation energy.

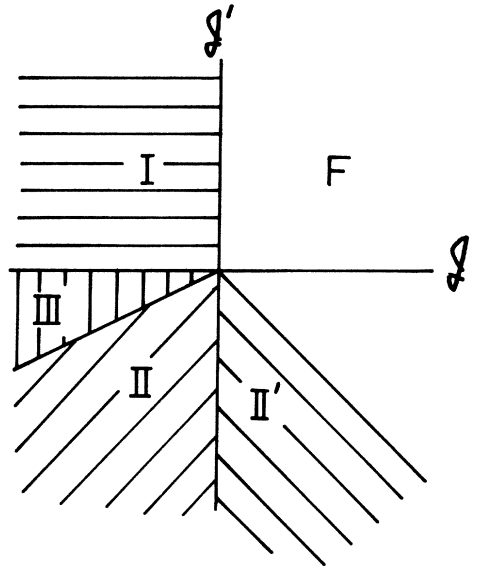

FIG. 11. Magnetic structures determined by the exchange constants and magnetization process in the fcc Ising system. $\mathcal{J}$ and $\mathcal{J}'$ are the exchange constants between nearest and second-nearest neighbors, respectively. F shows the ferromagnetic state, I the first-kind ordering with two-step magnetization, II and II' the second-kind ordering with three-step magnetization and a one-step one, respectively, and III the third-kind ordering with four-step magnetization.

The magnetization process is divided into four cases, I, II, II', and III, depending on both the sign and magnitude of $\mathcal{J}$ and $\mathcal{J}'$, where the second-kind ordering is separated into two cases, II and II'. The magnetization curves in cases II and II' show a three-step jump and a one-step jump, respectively, and the magnetization curve in case III shows a four-step jump. These characteristics do not appear for the bct $ErRh_4B_4$ crystal.

The magnetization process in the first-kind ordering is predicted to show a two-step jump, where the magnetic structure with magnetization of $M_0/2$ is expected as an intermediate state. This is just the case of bct $ErRh_4B_4$, when a magnetic field is applied along the easy-magnetization axis. In the following, under an assumption that the antiferromagnetic structure of bct $ErRh_4B_4$ belongs to the first-kind ordering, we explain the experimental results on the magnetization.

In Fig. 12 are shown the proposed magnetic structures of bct $ErRh_4B_4$, where the crystal structure is the same as in Fig. 1(a). Figures 12(a), 12(b), 12(c), and 12(d) represent the magnetic structures of the AF, I_1, I_2, and CF states, respectively (see Fig. 9). Figure 12(a) corresponds to the first-kind antiferromagnetic ordering in the fcc lattice in which the ferromagnetic ordered [010] planes exist. I_1 and I_2 shown in Figs. 12(b) and 12(c) appear as the ferrimagnetic state for H||[100] and H||[010], respectively, where the small energy difference of the magnetic anisotropy between the [100] and [010] axes is considered as described before. In the I_1 structure, antiferromagnetical-

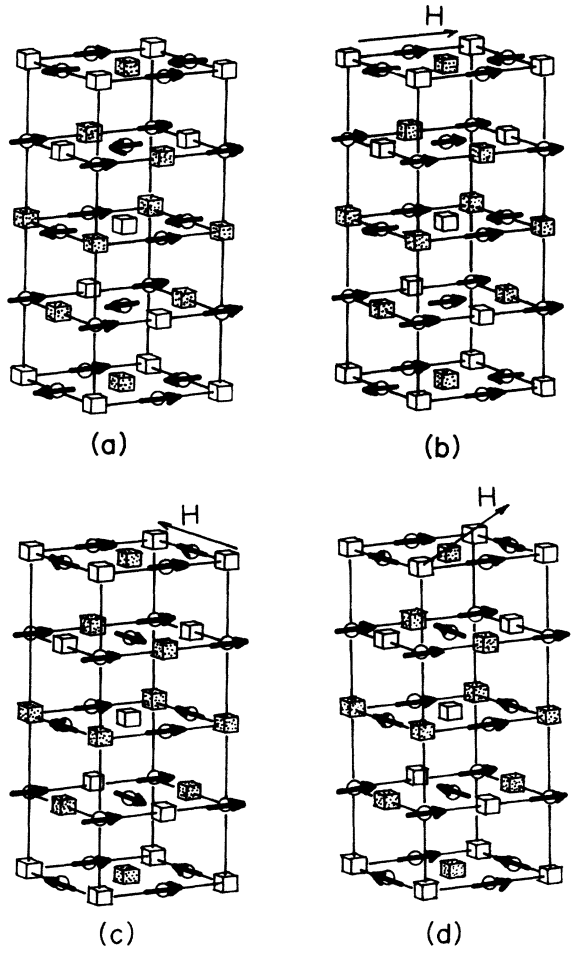

FIG. 12. Magnetic structures of bct $ErRh_4B_4$, (a) the antiferromagnetic structure, (b) and (c) the intermediate ferrimagnetic structures for H||[100] and H||[010], respectively, and (d) the canted ferromagnetic structure for H||[110].

ly and ferromagnetically ordered c planes are alternatively stacked along the c axis. In the I_2 structure a half of all the Er spins array parallel to the applied field and the rest perpendicular to the applied field. In the canted ferromagnetic structure in Fig. 12(d) for H||[110], half of all the Er spins arrange along the [100] axis and the rest along the [010] axis. These magnetic structures should be checked by the neutron-diffraction study, but we proceed through the free-energy analysis on the basis of magnetic structures shown in Fig. 12.

E. Magnetic free-energy estimation and magnetization process of bct $ErRh_4B_4$

In this section magnetic free energy is calculated on the basis of the magnetic structures, as shown in Fig. 12, which were derived from the four-sublattice model and the Kanamori theory[18] on the cubic Ising spin system. Using Eq. (3), the magnetic free energy for H||[100] in the four-sublattice model at $T=0$ in the AF, I_1, and F states is written as follows:

$$E_{AF}=-N(2|\mathcal{J}|+3\mathcal{J}')(g_J-1)^2J^2\,, \tag{7}$$

$$E_I=-N(3\mathcal{J}')(g_J-1)^2J^2-N\mu(H+2\pi M_0/3)/2\,, \tag{8}$$

and

$$E_F=-N(-6|\mathcal{J}|+3\mathcal{J}')(g_J-1)^2J^2 - N\mu(H+4\pi M_0/3)\,, \tag{9}$$

where N is the number of Er spins. Note that Eqs. (7), (8), and (9) include the same terms on $\mathcal{J}'$ from the second-nearest neighbors and then these terms do not contribute to the energy difference among three states. The magnetization always shows a two-step jump, irrespective of the magnitude of $\mathcal{J}$ and $\mathcal{J}'$ values, though the conditions $\mathcal{J}<0$ and $\mathcal{J}'>0$ must be fulfilled for the stability of the first-kind ordering. In this model we always obtain $H_3=3H_1$. Because in our experimental result $H_3\simeq 2.4H_1$, there is a small difference between the calculation and the experimental result.

In bct $ErRh_4B_4$, Er ions are slightly distorted from the fcc lattice and Rh_4B_4 clusters do not form the fcc lattice in a rigorous way. It should be noticed in Fig. 12(a) that the distance between the nearest Er ions in the same c plane which have spins of opposite directions is different from that between Er ions in neighboring c planes which have spins of the same direction. We divide $\mathcal{J}$ into $\mathcal{J}_1$ and $\mathcal{J}_2$ in order to shrink the difference between the calculated and the experimental results, where $\mathcal{J}_1$ and $\mathcal{J}_2$ are the exchange constants between the nearest neighbors in the same c plane and those between the neighboring c planes, respectively. The magnetic free energy for H||[100] in the AF, I_1, and F states is rewritten as follows:

$$E_{AF}=-N(2|\mathcal{J}_1|+3\mathcal{J}')(g_J-1)^2J^2\,, \tag{10}$$

$$E_I=-N(3\mathcal{J}')(g_J-1)^2J^2-N\mu(H+2\pi M_0/3)/2\,, \tag{11}$$

and

$$E_F=-N(-2|\mathcal{J}_1|-4|\mathcal{J}_2|+3\mathcal{J}')(g_J-1)^2J^2 - N\mu(H+4\pi M_0/3)\,, \tag{12}$$

where the values of $g_J=1.2$ and $J=\frac{15}{2}$ are used and $M_0=450$ Oe is obtained from the saturated magnetization value for the [100] direction (Fig. 4).[19].

$|\mathcal{J}_1|$ and $|\mathcal{J}_2|$ are calculated under the condition that E_{AF} is equal to E_I at H_1 and E_I is equal to E_F at H_3. Thus $|\mathcal{J}_1|$ and $|\mathcal{J}_2|$ are obtained to be ~ 86 mK and ~ 72 mK, respectively.

The free energy obtained for each state relative to the AF state is shown as a function of magnetic field in Fig. 13. As seen in this figure the AF state is stable below H_1, and the I_1 state becomes stable between H_1 and H_3 and then the F state becomes stable above H_3. The magnetization curve with the two-step jump is shown by the solid line in the lower part of Fig. 13.

Magnetic free energy for the CF state is given as follows, where a magnetic field is applied along the [110] axis:

$$E_{CF}=-N(-2|\mathcal{J}_2|+3\mathcal{J}')(g_J-1)^2J^2 - N\mu(H+4\pi M_0/3\sqrt{2})/\sqrt{2}\,. \tag{13}$$

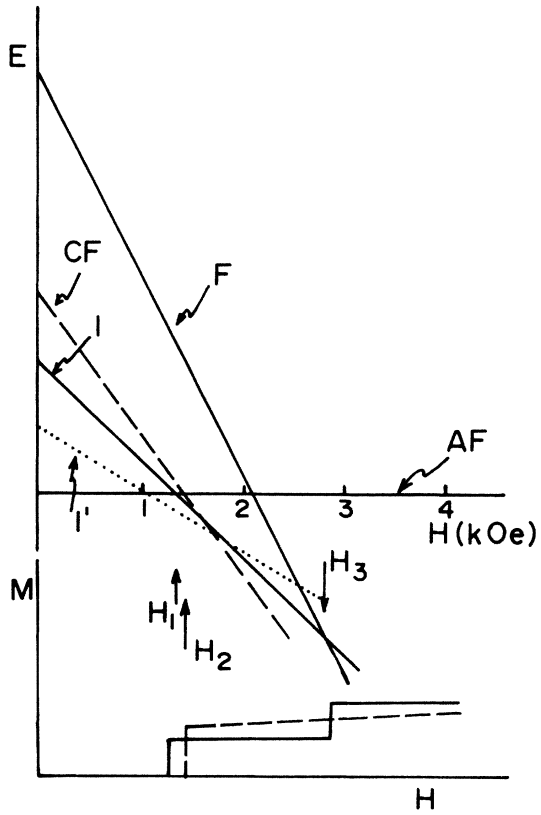

FIG. 13. Magnetic field dependence of the magnetic free energy of bct $ErRh_4B_4$ for each magnetic state for H||[100], shown by the solid line, and H||[110], shown by the dashed and dotted lines. The lower part shows the corresponding magnetization curves. The solid curve and the dashed curve show the magnetizations for H||[100] and H||[110], respectively.

The H_2 value calculated from Eq. (13) by use of the obtained values of $|\mathcal{J}_1|$ and $|\mathcal{J}_2|$ is in agreement with the experimental result that H_2 is a little higher than H_1. The corresponding magnetization curve for H||[110] is shown by the dashed line in the lower part of Fig. 13.

Since $\mathcal{J}'$ value cannot be determined in this analysis, $\mathcal{J}'$ is estimated from T_N by use of the molecular field approximation as follows:

$$T_N=(g_J-1)^2J(J+1)(4|\mathcal{J}_1|+6\mathcal{J}')/3\ . \tag{14}$$

In Eq. (14), $\mathcal{J}'$ is estimated to be ~ 60 mK. This positive value is consistent with the stability condition of the first-kind ordering.

Finally we must discuss the possibility of an appearance of the intermediate state with $M_0/2\sqrt{2}$,I' for H||[110] (see Fig. 9). The magnetic field dependence of the free energy of the I' state is also shown in Fig. 13 (dotted curve). The I' state can exist in a very narrow field range. However, such a structure is not observed in our experiment; only the direct phase transition from the AF state to the CF state appears. It should be noted that this narrow field range corresponds to that of magnetization anomaly, where magnetization decreases once just below H_2. As mentioned briefly in the preceding section, this phenomenon was interpreted as a kind of interplay between superconductivity and magnetism;[16] that is, the entrance of the vortices is suppressed by an increase of the vortex core energy due to the precursor effect in the metamagnetic transition. We would like to point out that the reason why this I' structure cannot be observed may be due to the existence of such an interplay. Therefore, if the sample shows no superconductivity, there is a possibility of observing a two-step jump for H||[110].

VI. CONCLUSION

We have succeeded in preparing a bct $ErRh_4B_4$ single crystal which is an antiferromagnetic superconductor. The sample has $T_c=7.80$ K and $T_N=0.65$ K. The c axis is found to be the hard-magnetization direction. The large fourfold magnetic anisotropy in the tetragonal c plane was observed in the superconducting paramagnetic state. The magnetization curve below T_N shows a two-step jump at H_1 and H_3, in the case of H||[100] and H||[010], and shows a one-step jump at H_2 in the case of H||[110]. The magnetization process below T_N in the c plane is understood as metamagnetism. The jumps at H_1 and H_3 correspond to the phase transition from the antiferromagnetic to the ferrimagnetic state and from the ferrimagnetic to the induced ferromagnetic state, respectively. The jump at H_2 corresponds to the phase transition from the antiferromagnetic to the canted ferromagnetic state. These three transitions at H_1, H_2, and H_3 are accompanied by hysteresis for increasing and decreasing fields, indicating a first-order phase transition. Furthermore, it is found that the ferrimagnetic state as well as the canted ferromagnetic state coexist, respectively, with superconductivity in bct $ErRh_4B_4$.

In order to explain the magnetization process, the magnetic free energy of bct $ErRh_4B_4$ is calculated. In the calculation, correction of the interplaying energy between superconductivity and magnetism is roughly made. The magnetization process below T_N can be explained by the four-sublattice model in which the fourfold magnetic anisotropy is taken into account. The antiferromagnetic structure expected from the magnetization process is proposed, being based on Kanamori theory. The antiferromagnetic structure corresponds to the first-kind ordering in the fcc lattice. The unique magnetic structure, we think, which is characteristic of the fourfold magnetic anisotropy is proposed as an intermediate state. However, it is strongly recommended that a neutron-diffraction study on a single crystal be made in order to determine the precise magnetic structure.

ACKNOWLEDGMENTS

We would like to thank Professor M. Tachiki and Professor S. Maekawa for valuable discussions. One of the authors (H.I.) was supported by a Grant-in-Aid for Encouragement of Young Scientists from the Ministry of Education, Science and Culture, Japan.

[1]B. T. Matthias, E. Corenzwit, J. M. Vandenberg, and H. E. Barz, Proc. Natl. Acad. Sci. USA **74**, 1334 (1977).

[2]For a review, see *Superconductivity in Ternary Compounds II,* Vol. 34 of *Topics in Current Physics,* edited by M. B. Maple and Ø. Fischer (Springer, Berlin, 1982).

[3]W. A. Fertig, D. C. Johnston, L. E. DeLong, R. W. McCallum, M. B. Maple, and B. T. Matthias, Phys. Rev. Lett. **38**, 987 (1977).

[4]S. K. Sinha, G. W. Crabtree, D. G. Hinks, and H. Mook, Phys. Rev. Lett. **48**, 950 (1982).

[5]M. Tachiki, A. Kotani, H. Matsumoto, and H. Umezawa, Solid State Commun. **31**, 927 (1979).

[6]E. I. Blount and C. M. Varma, Phys. Rev. Lett. **42**, 1079 (1979).

[7]H. Iwaski, M. Isino, K. Tsunokuni, and Y. Muto, J. Magn. Magn. Mater. **32**, 521 (1983).

[8]D. C. Johnston, Solid State Commun. **24**, 699 (1977).

[9]H. Iwasaki, M. Isino, and Y. Muto, Physica **108B**, 759 (1981).

[10]H. C. Hamaker and M. B. Maple in, *Ternary Superconductors* (North-Holland, Amsterdam, 1981), p. 213.

[11]R. Knauf, A. Thomä, H. Adrian, and R. L. Johnson, Phys. Rev. B **29**, 2477 (1984).

[12]D. C. Johnston, Solid State Commun. **42**, 453 (1982).

[13]H. Iwasaki and Y. Muto, following paper, Phys. Rev. B 33, 4680 (1986).

[14]H. Iwasaki, M. Ikebe, and Y. Muto, in *Proceedings of the International Conference LT 17 (1984),* edited by U. Eckern, A. Schmid, W. Weber, and H. Wühl (North-Holland, Amsterdam, 1984), p. 87.

[15]H. Iwasaki, M. Ikebe, and Y. Muto, in *Proceedings of the International Conference LT 17 (1984),* edited by U. Eckern, A. Schmid, W. Weber, and H. Wühl (North-Holland, Amsterdam, 1984), p. 89.

[16]H. Iwasaki, M. Tachiki, M. Ikebe, and Y. Muto, Solid State Commun. **51**, 879 (1984).

[17]J. S. Smart, Phys. Rev. **52**, 968 (1952).

[18]J. Kanamori, Prog. Theor. Phys. **35**, 16 (1966).

[19]It is difficult to explain both the absolute value and the anisotropy of the magnetization curves of bct $ErRh_4B_4$ above 1.7 K with the crystalline electric field Hamiltonian for Er^{3+} only. This problem is under consideration. In this paper we use the values of g_J and J for free Er^{3+} and the magnetic moment determined by the experiment.